Changes in *r*-process abundances at late times

R. Surman[1] and J. Engel[2]
[1]*Department of Physics, Union College, Schenectady, New York 12308*
[2]*Department of Physics and Astronomy, CB3255, University of North Carolina, Chapel Hill, North Carolina 27599*
(Received 7 March 2001; published 22 August 2001)

We explore changes in abundance patterns that occur late in the *r* process. As the neutrons available for capture begin to disappear, a quasiequilibrium funnel shifts material into the large peaks at $A=130$ and $A=195$, and into the rare-earth ''bump'' at $A=160$. A bit later, after the free-neutron abundance has dropped and beta decay has begun to compete seriously with neutron capture, the peaks can widen. The degree of widening depends largely on neutron-capture rates in a few nuclei near closed neutron shells and relatively close to stability. We identify particular nuclei whose capture rates should be examined experimentally, perhaps at a radioactive beam facility.

DOI: 10.1103/PhysRevC.64.035801 PACS number(s): 26.30.+k

I. INTRODUCTION

The *r* process, which synthesizes roughly half the elements with atomic mass number $A>70$, proceeds through neutron capture and beta decay [1–3]. Through most of the process, we know, capture is much faster than beta decay, so that very neutron rich and unstable nuclei are temporarily created before disappearing as the process peters out. The question of where the nucleosynthesis occurs, however, is still unanswered. An evacuated bubble expanding behind a supernova shock wave is a promising candidate for the site, but not yet the clear choice. The scenario is more convincing if the initial expansion is very rapid [4], but simple models of fast adiabatic expansion [5] imply that the neutron capture must finish in less than a second. In traditional simulations, where capture must often wait for a nucleus to beta decay, it takes two or three times longer to make the heaviest elements.

Simulations from, e.g., Ref. [5] demonstrate that the entire process can take place quickly if neutron capture populates nuclei farther from stability (and thus shorter lived) than usually thought. Despite initially forming at lower Z and A than traditional work suggests, the simulated abundance peaks end up at the right spots. The apparent reason is that nuclei in the peak move up quickly in Z near the end of the *r* process, when the supply of free neutron begins to run out but before neutron capture completely stops. But how do peaks maintain themselves during this late time, as beta decay drives each nucleus at a different rate towards stability? This question is actually more general than the rapid-expansion scenario; a quick move towards stability while the neutron abundance drops, though most dramatic if the path is initially very far away, in fact characterizes all bubble *r*-process simulations that produce something like the correct abundance distribution. And the question is linked to a broader issue: the significance of neutron capture once its rate has slowed down so that it must compete with beta decay. What happens if the capture rates at that time are faster or slower than we think? In which nuclei do capture rates have the largest effects on final abundances, and can the rates there be measured? These are the kinds of issues we address here.

The late stages of neutron capture and beta decay in the *r* process are much different from what precedes them. When the neutron-to-nucleus ratio R is much larger than 1, equilibrium between neutron capture and photodisintegration is a good approximation; the ''path'' consisting of the most abundant isotopes for each element Z is far from stability and moves relatively slowly. The term ''steady state'' is sometimes used to refer to this period, which ends when the neutron-to-seed ratio R falls below a few. To see what happens next, we note that the neutron separation energies along the path in $(n,\gamma)\leftrightarrow(\gamma,n)$ equilibrium are related to the neutron number density n_n, which is proportional to R for slowly changing matter densities, by

$$S_n \approx -kT \ln\left\{\frac{n_n}{2}\left(\frac{2\pi\hbar^2}{m_n kT}\right)^{3/2}\right\}, \tag{1}$$

where m_n is the neutron mass. When R drops below about 1, a nucleus on the path that beta decays can no longer capture enough free neutrons to return to the path so that the path itself must move instead, inwards to higher neutron separation energy. The increased average neutron binding makes photodisintegration less effective, which in turn reduces the number of free-neutrons still further, in accordance with Eq. (1). This dynamic feeds on itself, causing R to drop exponentially and the *r*-process path to move quickly towards stability. Soon R becomes so small that $(n,\gamma)\leftrightarrow(\gamma,n)$ equilibrium begins to fail, and beta decay moves a good fraction of nuclei away from the path. Eventually, beta decay becomes faster than neutron capture and all remnants of $(n,\gamma)\leftrightarrow(\gamma,n)$ equilibrium vanish. The inability of equilibrium to maintain itself on the time scale of beta decay is usually called ''freeze-out.''

To answer the questions about peak evolution and the significance of neutron capture at late times, we focus on two competing effects. The first, which dominates just as R falls below 1, when $(n,\gamma)\leftrightarrow(\gamma,n)$ equilibrium still holds well, is a funneling of material into moving peaks, most notably the small rare-earth peak [6], but also the larger peaks at $A=130$ and 195. As time passes, the funnel fights an increasing tendency for the peaks to spread because beta decay and beta-delayed neutron emission compete harder with neutron

capture. The interplay of funneling and spreading will imply that uncertain neutron capture rates, which are irrelevant as long as $(n,\gamma)\leftrightarrow(\gamma,n)$ equilibrium holds, become important fairly near stability, and should be determined there more precisely.[1]

We support our contentions with simulations of the neutron-capture part of the *r* process. In most, we explore late times without worrying about a fast *r* process. We assume an exponential decay of temperature $T_9=T_9(0)e^{-t/\tau}$ and density $\rho_5=3.3T_9^3/S$ (where ρ_5 is in units of 10^5 g/cm^3, and the entropy *S*, in units of *k*, is held constant at 300) with a relatively slow time scale of $\tau=2.8$ s, the same as in Ref. [7]. We start with the post-alpha-process distribution of Ref. [7] and a neutron-to-seed ratio of 70, and we vary the initial temperature. What we call our ''standard simulation'' uses an intial temperature of $T_9(0)=1.5$. In Sec. III, we worry more about a fast *r* process and therefore use different conditions. We do this in two ways: the first is to use the same temperature and density dependence as described above, but a greater initial density (and thus a lower and probably unrealistic entropy: $S=5$, for which we compensate by increasing the neutron-to-seed ratio to 100). The faster neutron capture at high density pushes the path farther from stability and leads to the formation of the $A=195$ peak and the exhaustion of free neutrons in only tenths of a second. The second way is to use the conditions of Ref. [5] where the temperature and density drop with a time scale of $\tau=50$ ms, according to $T_9=T_9(0)\tau/[\tau+(e-1)t]$ [with an initial temperature $T_9(0)=2.6$ and a dependence of ρ on *T* and *S* similar to that above], and then level off at low values ($T_9<1$, $\rho_5<10^{-3}$). The resulting drop in photodissociation rates again moves the path farther from stability, and the $A=195$ peak forms in under a second. All our simulations use nuclear masses from Ref. [8] and beta-decay rates from Ref. [9].

The rest of this paper is organized as follows: In Sec. II, we discuss the action of funneling and spreading in the formation of the rare-earth element bump. Section III applies the same ideas to the large peaks, with emphasis on the change in the peak's location and width as the path moves. The most important results appear in Sec. IV, which discusses neutron capture near the peaks and isolates particularly important rates that should be measured. Section V is a conclusion.

II. FUNNELING AND SPREADING IN THE RARE-EARTH REGION

Reference [6] presented the basic dynamics of the near-freeze-out funnel. It concluded that for much of the time when $R<1$, the system is still nearly in $(n,\gamma)\leftrightarrow(\gamma,n)$ equilibrium, even as the path moves inwards. A kink at $N=104$ and 106 soon develops (or grows stronger) when the path approaches a deformation maximum, which acts like a miniature closed shell. The nuclei near the bottom of the kink are further from stability than those at the top and thus have shorter beta-decay lifetimes (see Fig. 3 from Ref. [6], which shows the path together with contours of constant beta-decay lifetime). The rate at which the path moves is governed by the average beta-decay lifetime along the path, which typically corresponds to a nucleus in the kink. The nuclei below the kink have shorter lifetimes than this overall average, and tend to beta decay before the path moves, then capture neutrons in an attempt to stay in equilibrium along the path. The nuclei above the kink have longer lifetimes and so do not usually beta decay before the path moves, instead photodissociating to keep up with a path that is moving away from them. Eventually the neutron abundance is so low that neutrons are essentially transferred from nuclei that photodisintegrate to those that capture. The net result is that nuclei both near the bottom and top of the kink funnel into it as the path moves, leading to a peak in the final abundances, whether or not one exists before $R=1$.

Another process, this one not discussed in Ref. [6], acts to weaken the funnel. As *R* drops below 1, so does the rate at which neutrons are captured, since it is proportional to the neutron abundance. As a result, a nucleus in or near the kink will not always have time to capture neutrons after it has beta decayed; it may first undergo another beta decay and move away from the path of greatest abundances. Nuclei can emit neutrons following beta decay, moving them still further from the path. Thus, part of the growing peak begins to seep to lower neutron number *N*. Together with material from above the peak moving down in *N*, this spreading acts to wash out the peak in both *N* and *A*.

Funneling and spreading counter one another, but as noted in the Introduction, the two mechanisms reach their most effective points at different times. Close to $R=1$, when the path begins its inward trek, there are still enough neutrons so that spreading is slow and the funnel dominates. At very late times, by contrast, *R* is so small that $(n,\gamma)\leftrightarrow(\gamma,n)$ equilibrium is seriously compromised and spreading is substantial. Eventually, neutron capture becomes slower than beta decay and the system freezes entirely out of equilibrium. After that capture essentially stops and the only thing affecting the abundance distribution vs *A* is some final spreading from delayed neutron emission. Beta decay without emission continues to move nuclei away from the equilibrium path, altering the distribution in *N*, but has no effect on abundances plotted vs *A* (as they usually are).

Our simulations make all these statements concrete. Figure 1 compares the results of our ''standard'' simulation described in the introduction with the measured abundances in the rare-earth region as a function of *A*, showing the existence of a rare-earth peak, in reality and in the simulation. The simulated peak clearly relies on a kink that develops in the path because of the deformation maximum but, as argued in Ref. [6], the mere existence of a kink is not sufficient to fully produce such a peak; it achieves its full size only because of funneling. To see in more detail how the peak builds, we plot in Fig. 2 the number of nuclei in three regions of *N*—that just below the peak's location prior to freeze-out ($N=95$ to 101), that including the peak ($N=102$ to 106),

[1]If the *r* process is somehow terminated by a very rapid falloff in temperature and density, rather than the exhaustion of neutrons, the evolution of abundances at late times is different and these considerations are not relevant.

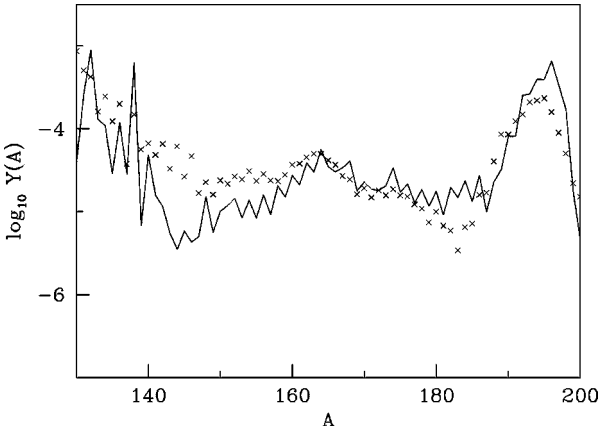

FIG. 1. Predictions of our standard simulation (solid line) for the final abundances of *r*-process nuclides vs atomic mass number *A*, and the measured abundances (crosses) scaled to the simulation. Note the peaks in the rare-earth element region near $A=160$.

and that just above the peak ($N=107$ to 113)—as a function of time for the run just discussed. The two vertical lines mark the points at which $R=1$, and at which beta decay and capture rates are equal in the rare-earth region, causing the complete freeze-out of $(n,\gamma)\leftrightarrow(\gamma,n)$ equilibrium there. The bump develops, and then actually starts to shrink as material moves to higher *A* early in the process. But just before $R=1$, as the path begins its inward move, it grows again. As noted above, photodisintegration is the dominant reaction above the bump in *N* and beta decay the important reaction below, so that material on both sides of the bump shifts inwards. After one or two tenths of a second, spreading begins in earnest; nuclei in the bump move slowly to lower *N* and material moves down from above to fill the trough above the peak, so that the abundance outside the peak starts to increase. To the right of the second vertical line, only beta decay (sometimes with the emission of neutrons) occurs, so that material is shifted downwards as the bump itself moves to lower *N*.

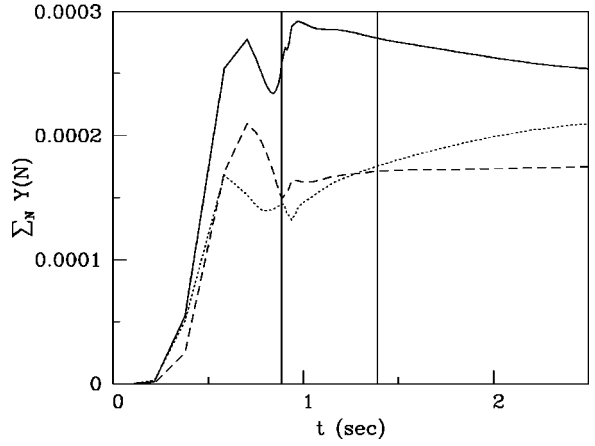

FIG. 2. Results of our standard simulation for the total abundances in the regions just below the pre-freeze-out peak (dotted line), in the pre-freeze-out peak (solid line), and just above the pre-freeze-out peak (dashed line) as a function of time. A drop in peak material is suddenly reversed when the neutron/nucleus ratio *R* nears 1, a point indicated by the first solid vertical line. The second solid vertical line indicates the time of freeze-out in the rare-earth region.

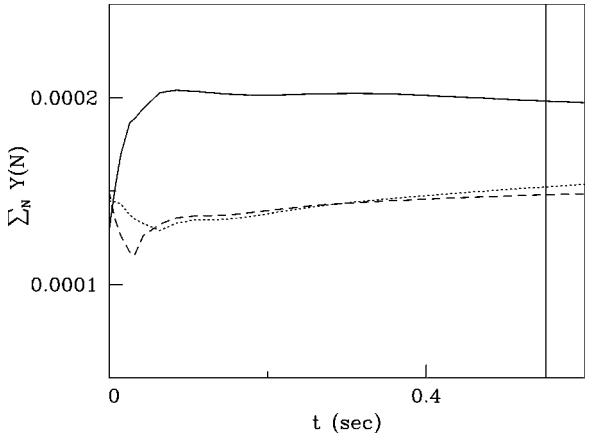

FIG. 3. The same as Fig. 2, except that the abundances have been adjusted when $R=1$ so that the three regions all contain the same total. Now $R=1$ occurs at $t=0$ and the solid vertical line indicates the time of freeze-out. The formation of a peak here is due solely to funneling.

Although the brief region during which funneling dominates is evident in this figure, one may wonder whether the peak could form even if it was absent during the steady-state phase along the path far from stability when $R>1$. In Ref. [6] we argued that was the case, and Fig. 3 here provides more evidence. To make the figure we took the run discussed in Figs. 1 and 2 and adjusted the abundances at $R=1$ so that the three regions of *N* were equally populated. We then let the run proceed starting from $R=1$; the rare-earth bump still formed. Figure 3 clearly shows that funneling in the first tenth of a second or so is responsible. (Some material is brought in from outside the range of the plot.) Here as before, later times show effects of spreading and the post-freeze-out shifting of material downwards in *N*.

III. FUNNELING AND SPREADING IN THE FORMATION OF THE $A=195$ PEAK

The fast *r* process of Ref. [5] relies on the formation of large peaks farther from stability than usually thought. Simulations from Ref. [5] show that the fast process works but do not explain how. Why should a peak that forms early at, e.g., $N=126$, remain there when the path moves as neutrons are exhausted? In more traditional simulations, when the path is assumed not to move before freeze-out, the usual explanation for peak buildup is approximate ''steady beta flow,'' which results in the longest lived nuclides building up the most. But this kind of buildup takes at least as long as the lifetime of the longest-lived nucleus, and the inward motion of the path we are discussing here takes much less time. Something like steady flow therefore cannot be responsible for the existence of the peak at its final location in Ref. [5]. What is? The answer is a funneling phenomenon similar to that we have already discussed, though slightly more complicated because instead of a kink we now have a long ladder of $N=126$ isotopes populated at any given time.

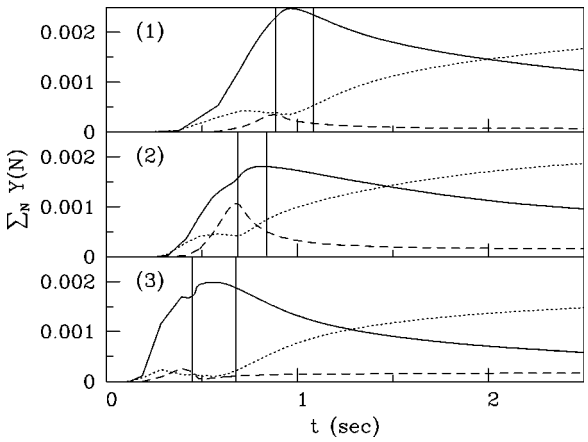

FIG. 4. Total abundances in the regions just below $N=126$ (dotted line), right around $N=126$ (solid line), and just above $N=126$ (dashed line) as a function of time for the three types of simulations discussed. Simulation (1) is the standard simulation, (2) uses the conditions of Ref. [5], and (3) is the standard simulation at much lower entropy.

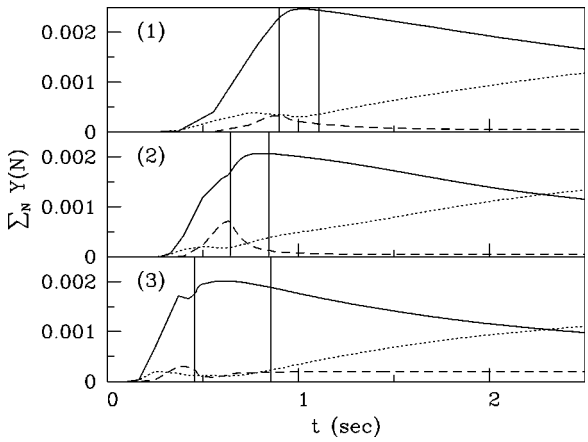

FIG. 5. Same as Fig. 4, but with simulations using a newer set of neutron-capture rates from Ref. [12].

As already noted, the speed at which the path moves inward after $R<1$ is given by the average rate of beta decay along the path. This average rate tends to occur along nuclei in the middle of the ladders at $N=82$ and 126. Thus the nuclei below them in N decay, and then capture into the peak as long as the funnel operates efficiently. A decay followed by a capture moves a nucleus up in Z, so material at the bottom of the ladder moves into the center of the ladder as the funnel proceeds. Further up the ladder, nuclei neither capture nor photodissociate, since the path continues to run through these nuclei even as it moves toward stability. Instead they simply beta decay, but more slowly than nuclei at the bottom of the ladder. The result is that the entire ladder shortens as the bottom moves up faster than the top. Above the ladder, for N just above 82 or 126, nuclei with slower beta-decay rates photodissociate into the peak, adding material just as in the rare-earth region. These dynamics combine to move the peak up in A at the same time as they heighten and narrow it. Though the large peaks clearly form during the steady-state phase of the r process, when $R \gg 1$, they are shaped and moved at later times as just described.

These dynamics, however, can sometimes be masked by spreading. Whether or not they are depends on the temperature and density of the environment and on nuclear properties. Figure 4 shows the funneling and spreading of material around the $A=195$ peak in our standard simulation as well as the two faster simulations described in the introduction. As in Fig. 2, we plot sums of abundances in three regions of N—below the peak ($N=110$–123), within the peak ($N=124$–126), and above the peak ($N>126$)—as a function of time. In each case, the peak forms when $R>1$, but continues to grow for the few tenths of a second following $R=1$. Much of this material comes from the photodissociation of material above the peak (dashed line in each plot). At later times, spreading takes over as material in the peak beta decays to lower N. The onset and rate of spreading depends on how fast the neutrons are depleted after $R<1$, which in turn depends on the temperature and density. For a simulation at high density, as in part (3) of Fig. 4, neutrons disappear very rapidly when $R<1$, and so in a short time beta decay and beta-delayed neutron emission win out completely over neutron capture. When the density and temperature drop quickly, as in part (2) of the figure, neutrons disappear more slowly. As a result, neutron capture competes with beta decay over a longer period of time, delaying the full onset of spreading. Nonevironmental factors can also affect the balance between funneling and spreading. In anticipation of our discussion of neutron capture in Sec. IV, we run simulations with the same three sets of conditions but a newer set of calculated neutron-capture rates, from Ref. [12]. Figure 5 shows the funneling and spreading of material in these simulations; the latter is less effective than in Fig. 4. We expand on this point in the next section.

The way the peak moves and gets shaped in A can be seen in Fig. 6, which shows its time development in the three types of simulations. While the peak initially narrows some as discussed above, it soon spreads, so that the effect is barely visible. Figure 7 shows the same development but with the newer capture rates. Here the narrowing of the peaks is evident, and is not erased by spreading at later times. The shifting of the peak to higher A is apparent in both sets of plots, and is most pronounced in the faster simulations where the peak forms much further from stability.

IV. SIGNIFICANCE OF CAPTURE RATES

Funneling operates unhindered just a short time before $(n,\gamma)\leftrightarrow(\gamma,n)$ equilibrium falters and spreading sets in. As we saw in the last section, once spreading is important, neutron-capture rates become so too. They determine how likely a nucleus that has beta decayed is to return to the path before decaying again. Fast rates mean that $(n,\gamma)\leftrightarrow(\gamma,n)$ equilibrium hangs on longer and spreading is delayed. Thus, the ultimate degree of widening a peak experiences depends on neutron-capture rates. To illustrate this point, we run simulations of the three types discussed above with four different sets of calculated rates [2,10–12]. These sets were calculated with different models for nuclear masses, slightly

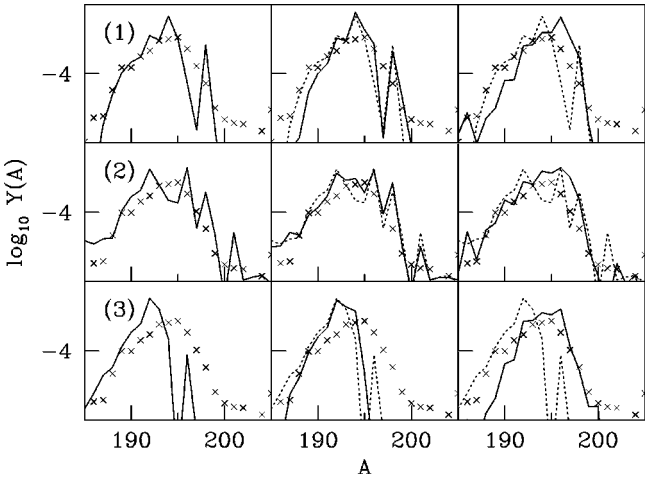

FIG. 6. The evolution of the 195 peak in late times for the three types of simulations, labeled as in Fig. 4. The first frame in each row shows the peak at $R\sim1$, the third frame shows the final abundances, and the second frame is taken from a time in between, when R is less than 1 but much larger than its value at freeze-out. For comparison, the dotted line in the second and third frames replots the abundances from the first frame. The scaled observed abundances are plotted as crosses.

different treatments of the dominant statistical capture, and different assumptions about the importance of direct capture. Not surprisingly, the rates can differ from one another significantly. Figure 8 plots the ratio of the smallest to largest rates as a function of N and Z. When we use these rates in simulations (though all with the same mass model [8]) we find variations in the final results for all values of A. We continue to focus on peaks, however, partly because the abundances are higher there than in neighboring regions, so differences are more significant, and partly because the differences in the left edge of the $A=195$ peak are particularly noticeable. As we already saw in the last section, and as Figs. 9 and 10 show in more detail, the peak does not spread very much when rates are fast near the $N=126$ closed shell. By contrast the slowest rates at these points cause the widest

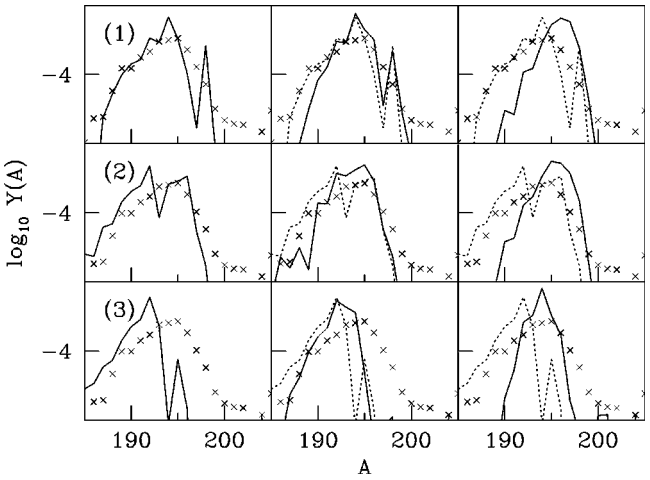

FIG. 7. Same as Fig. 6, but with simulations using a newer set of neutron-capture rates from Ref. [12].

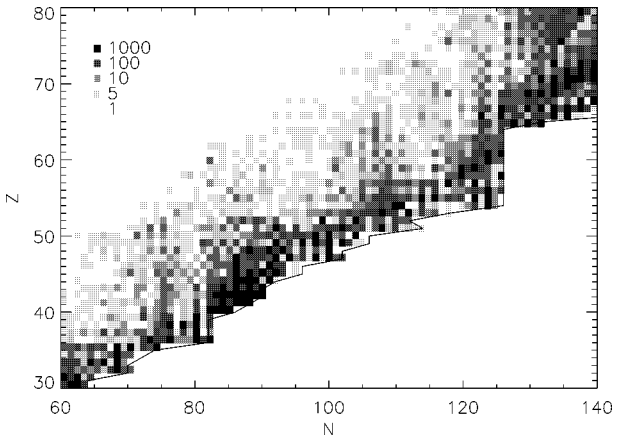

FIG. 8. For each N,Z the log of the ratio of the highest neutron-capture rate in our set [2,10–12] to the lowest. The darkest squares correspond to ratios greater than 1000, as indicated in the key.

final peaks. These effects, incidentally, are particularly significant for the Ref. [5] conditions, where $(n,\gamma)\leftrightarrow(\gamma,n)$ equilibrium falters earlier because of the rapid drop in temperature and density, so that capture rates become important sooner.

We can see the role of capture near the peak even more clearly by changing the rates only for N between 123 and 125. Figure 11 shows the results when those rates are multiplied by 10 or 100, or divided by 100. When the rates increase, funneling becomes stronger and spreading weaker as $(n,\gamma)\leftrightarrow(\gamma,n)$ equilibrium is partially restored. As a result, the final abundance peak at $A=195$ narrows.

It so happens that the nuclei at and just below closed shells are notoriously difficult to calculate [13]. Commonly used statistical methods may not be applicable for all those nuclei because of the low density of states at low energies [13,12]. Rates of direct capture, which also plays a role, are uncertain because we do not know how much isovector dipole strength lies low in nuclei far from stability. To determine the astrophysical parameters in the *r*-process environment, it is therefore important to measure the rates in these nuclei where possible. Of course most of them are out of

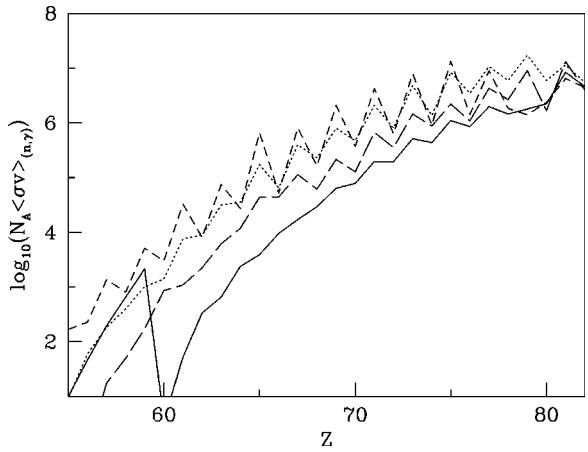

FIG. 9. The four sets of neutron-capture rates, plotted as a function of Z, for $N=124$ just below the closed neutron shell.

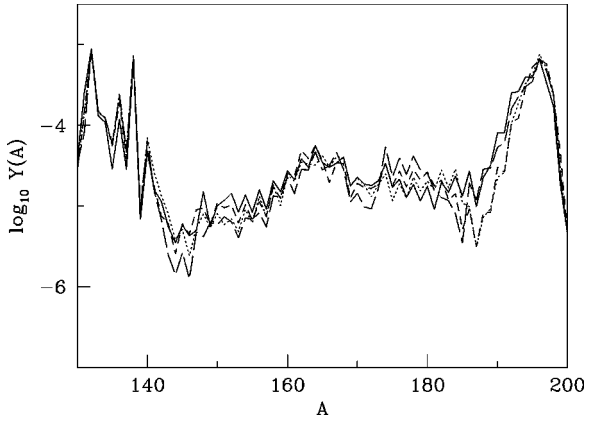

FIG. 10. Abundance curves from our standard simulation with the four sets of neutron-capture rates. Faster rates near the closed shell yield a narrower $A=195$ peak (note the left edge of that peak).

experimental reach for a long time to come. But the most important are actually relatively close to stability.

To show why this is, we make even more selective changes, now for just one or two values of Z, in the rates for N between 123 and 125. Figure 12 plots the root-mean-square difference between the abundance distribution (within our standard simulation) when these rates are increased by 100 and and when they are unaltered, as a function of time. *The ultimate degree of change depends strongly on which rates we change*. Altering those with $Z<69$ does little in the end because (a) these nuclei are farther from stability, where the system is closer to $(n,\gamma)\leftrightarrow(\gamma,n)$ equilibrium and capture rates are nearly irrelevant, and (b) any changes that do occur have time to be diluted by spreading. Altering those with $Z>72$ does not do much to the final abundance pattern because the system has nearly frozen out of equilibrium, making neutron capture irrelevant because its rate is so low. The nuclei for which changes do have large permanent effects lie between $Z=69$ and 72 (Tm, Yb, Lu, and Hf), and correspond to the rough location of the path just before full

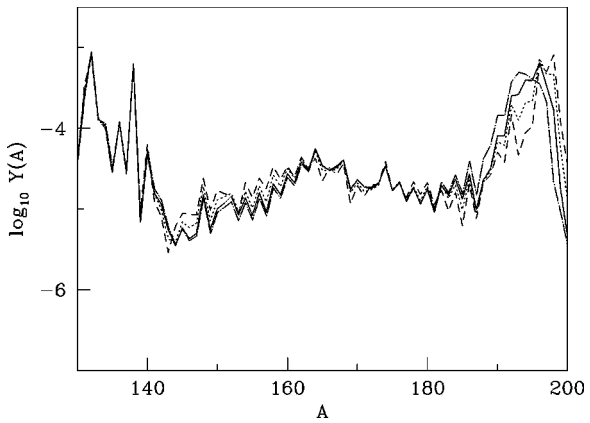

FIG. 11. Abundance curve when the capture rates for $N=123-125$ alone are changed. The solid line represents the results with the rates from Ref. [2], the dotted line represents the results when those rates are increased by 10, the dashed line represents the results when the rates are increased by 100, and the dot-dashed line represent the results when the rates are shrunk by 100.

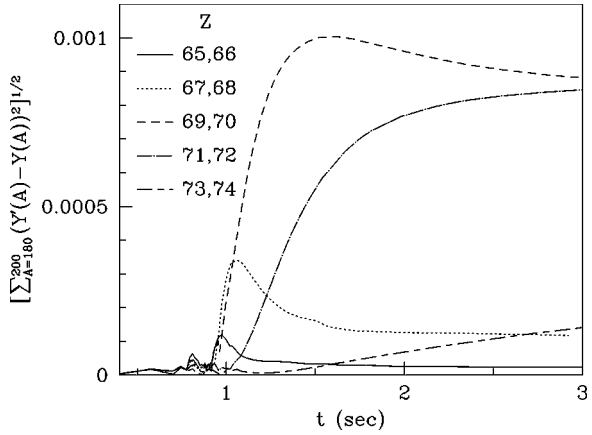

FIG. 12. Root mean square differences between the abundances with the rates of [2] and with those same rates everywhere except for a few nuclei with two values of Z and $N=123-125$ (those are multiplied by 100), as a function of time. We used the standard-simulation conditions. Each curve corresponds to increasing a different set of rates. The nuclei with the largest effect on the final abundances have $Z=69-70$ and $71-72$.

freeze-out, when neutron capture and beta decay compete on equal footing. Then dramatic differences in flow result from increasing the neutron-capture rates, differences that are not erased by any subsequent spreading. We see similar effects when the rates are decreased instead of increased. Figure 13 shows final abundance curves for a standard run with the rates of Ref. [2] and standard runs in which the capture rates of the nuclei with $Z=69-72$ and $N=123-125$ are increased by 10 and 100. The differences are significant. All these statements remain true both when we make wide variations in the initial temperature, initial density, and time scale in our simulations, and when we use the conditions of Ref. [5]. The reason is that in this range of Z, the calculated [9] beta-decay lifetimes of the $N=126$ nuclei increase from

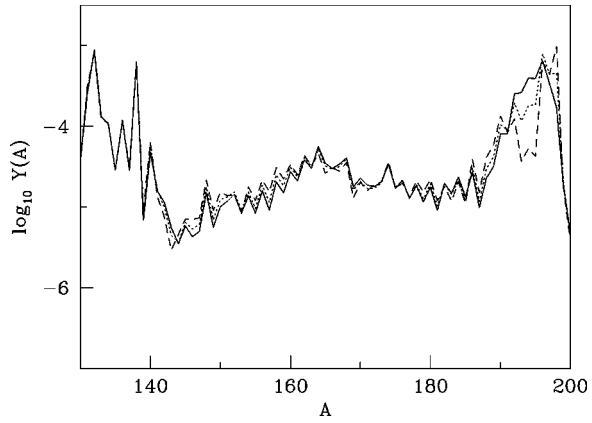

FIG. 13. Final abundance curves in the simulation yielding Fig. 12 when only the rates of nuclei with $N=123-125$ *and* $Z=69-72$ are increased, by factors of 1 (solid line), 10 (dotted line), and 100 (dashed line). Note the results of these simulations are nearly identical to those of Fig. 11; the largest changes to the final abundance distribution are due to the modification of the capture rates of just these 12 nuclei.

about 0.07 s to 4.2 s.[2] The moving path there slows down around the peak, giving the neutrons time to disappear through capture on nuclei in other regions. This happens whether in the time prior the path moves over a large distance (quickly at first, because of the fast beta decay rates far from stability) or over a shorter distance. Although it is theoretically possible for freeze-out to occur for $Z<69$, the resulting peak would almost certainly be too low in A to match the observed abundances.

The rates for these few nuclei are thus the ones on which the final *r*-process abundances depend most sensitively, and measuring the associated cross sections would be useful; with them we could better constrain the temperature and density during the *r* process. Unfortunately these nuclei are still far enough from stability that their cross sections may not be possible to measure, even partially through spectroscopic factors in transfer reactions with radioactive beams at RIA. A yield of about 10^4/sec is probably necessary for such experiments, while estimates [15] of production at a RIA ISOL facility indicate that Z must be about 77 before yields will become that large. But we can still approach the nuclei we are interested in, and see how measurements and calculations compare near the most critical region.

We are more fortunate in the rare-earth region because neutron-capture rates are faster there than near the $A=195$ peak, and freeze-out therefore occurs closer to stability. Figure 14 shows what happens when we selectively change the capture rates of nuclei just below the kink, with $N=102$–104, for particular values of Z. The nuclei with the strongest effect now have $Z=62$ and 63 (Sm and Eu). As before, the location of the most important nuclei is not very sensitive to initial *r*-process conditions. These nuclei are actually within RIA's reach. For the nucleus $Z=62$, $N=102$ (^{164}Sm), yields should be about 10^5/sec, for $Z=63$, $N=102$ (^{165}Eu) they should be about 10^6/sec, and for $Z=63$, $N=104$ (^{167}Eu) about 10^4/sec [15]. Experiments to study their capture cross sections are worth considering.

We have not discussed the $A=130$ peak in any detail. Our conclusions there are more limited because we do not reproduce the region below the peak very well. Abundances in that area are very sensitive to the outcome of the alpha process, which we do not simulate. Nonetheless we do get a peak at $A=130$ and generally find that varying the $N=79$–81 neutron-capture rates has the largest effect for $Z=48$–51 ($^{127-129}$Cd, $^{128-130}$In, $^{129-131}$Sn, $^{130-132}$Sb). RIA should be able to make enough of these isotopes to allow experiments.

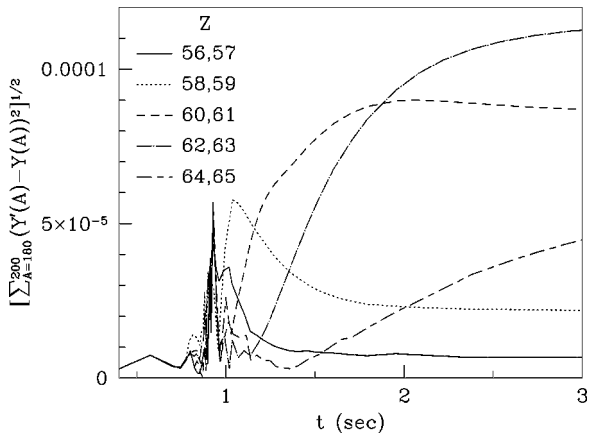

FIG. 14. Same as Fig. 12, except for the rare-earth region, where rates of nuclei with $N=102$–104 and particular values of Z are changed. The nuclei with the largest effect on the final abundances have $Z=62$–63.

V. CONCLUSION

For most of the *r* process, neutron-capture rates are irrelevant because they are fast enough to maintain equilibrium with photodisintegration. But at late times, the situation is different. Our investigation of funneling and spreading led us to identify particular nuclei relatively close to stability whose neutron-capture rates have significant effects on the shapes of peaks. It would be nice to have experimental information about these nuclei, even if indirect, e.g., spectoscopic factors through (d,p) neutron-transfer reactions. Measurements of the capture rates themselves in other nuclei closer to stability would also be useful; they would help tune models, which could then be better extrapolated to the important nuclei identified here. A full understanding of the *r* process would then be a little closer.

ACKNOWLEDGMENTS

We thank J. H. de Jesus, B. S. Meyer, M. Smith, and P. Tomasi for useful discussions. We were supported in part by the U.S. Department of Energy under Grant No. DE-FG02-97ER41019.

[2]When we replace these lifetimes with the more accurate and faster ones calculated in Ref. [14], we find only slight differences in Fig. 12.

[1] E. M. Burbidge, G. R. Burbidge, W. A. Fowler, and F. Hoyle, Rev. Mod. Phys. **29**, 547 (1957).

[2] J. J. Cowan, F.-K. Thielemann, and J. W. Truran, Phys. Rep. **208**, 257 (1991) is a review.

[3] B. S. Meyer, Annu. Rev. Astron. Astrophys. **32**, 153 (1994) is another review.

[4] Y.-Z. Qian and S. E. Woosley, Astrophys. J. **471**, 1331 (1996); R. D. Hoffman, S. E. Woosley, and Y.-Z. Qian, *ibid.* **482**, 951 (1997).

[5] C. Freiburghaus *et al.*, Astrophys. J. **516**, 381 (1999).

[6] R. Surman, J. Engel, J. R. Bennett, and B. S. Meyer, Phys. Rev. Lett. **79**, 1809 (1997).

[7] B. S. Meyer, G. J. Mathews, W. M. Howard, S. E. Woosley, and R. Hoffman, Astrophys. J. **399**, 656 (1992).

[8] P. Möller, J. R. Nix, W. D. Myers, and W. J. Swiatecki, At. Data Nucl. Data Tables **59**, 185 (1995).
[9] P. Möller and J. Randrup, Nucl. Phys. **A514**, 1 (1990).
[10] S. Goriely (unpublished).
[11] Institut d'Astronomie et d'Astrophysique CP226, Université Libre de Bruxelles, http://www-astro.ulb.ac.be/Html/ncap.html
[12] T. Rauscher and F.-K. Thielemann, At. Data Nucl. Data Tables **75**, 1 (2000); ftp://quasar.physik.unibas.ch/pub/tommy/astro/fits/957fit_frdm.asc.gz
[13] See S. Goriely, Phys. Lett. B **436**, 10 (1998); Astron. Astrophys. **325**, 414 (1997).
[14] J. Engel, M. Bender, J. Dobaczewski, W. Nazarewicz, and R. Surman, Phys. Rev. C **60**, 014302 (1999).
[15] See the RIA web page http://www.phy.anl.gov/ria/index.html